Three-Dimensional Enantiomeric Recognition of Optically Trapped Single Chiral Nanoparticles

Gabriel Schnoering,[1] Lisa V. Poulikakos,[2] Yoseline Rosales-Cabara,[1]
Antoine Canaguier-Durand,[3] David J. Norris,[2] and Cyriaque Genet[1,*]
[1]*ISIS and icFRC, University of Strasbourg and CNRS, 8 allée Gaspard Monge, 67000 Strasbourg, France*
[2]*Optical Materials Engineering Laboratory, ETH Zürich, 8092 Zürich, Switzerland*
[3]*Laboratoire Kastler Brossel, Sorbonne Université, CNRS, ENS-PSL University, Collège de France, 75005 Paris, France*

(Received 24 February 2018; published 10 July 2018)

We optically trap freestanding single metallic chiral nanoparticles using a standing-wave optical tweezer. We also incorporate within the trap a polarimetric setup that allows us to perform *in situ* chiral recognition of single enantiomers. This is done by measuring the S_3 component of the Stokes vector of a light beam scattered off the trapped nanoparticle in the forward direction. This unique combination of optical trapping and chiral recognition, all implemented within a single setup, opens new perspectives towards the control, recognition, and manipulation of chiral objects at nanometer scales.

DOI: 10.1103/PhysRevLett.121.023902

Artifical chiral nanostructures have opened new perspectives in the field of colloidal science, optics, and spectroscopy [1–3]. Chiral plasmonic nanostructures, for instance, have led to the possibility of enhancing chiroptical signals through the excitation of so-called superchiral electromagnetic fields [4–8]. New strategies proposed recently for preparing colloidal suspensions of chiral nano-objects have allowed fascinating experiments on active Brownian motions and have sparked strong activities [9–14]. In parallel, chiral structures interact specifically with chiral light fields, as seen, in particular, through the emergence of new types of optical forces recently described [15–20]. While such forces have only been probed experimentally at the micrometer scale [21,22], the outstanding chiroptical signatures associated with these new artificial chiral nano-objects could facilitate, despite their small sizes, the observation of such chiral optical forces on nanometer-sized objects.

To move toward manipulating chiral matter at nanometer scales, one crucial step is the spatial control of a single chiral nano-object in freestanding conditions. In this Letter, we develop an optical tweezer capable of trapping single chiral metallic nano-objects that diffuse in a fluidic cell. We demonstrate three-dimensional stable optical trapping of single artificial Au nanopyramids (NPys) in both enantiomeric forms. Simultaneously, the enantiomeric form of the trapped NPy is recognized through a far-field polarization analysis of the scattered light inside the trap, at the single-particle level. Our experimental strategy is grounded on fundamental concepts (conservation law of optical chirality and chiral scattering) that lead to new physical discussions, as exemplified in our use of chiral symmetries in the context of optical trapping. Our work shows how such concepts, which are at the core of many current debates and discussions, can turn operational in the experimental study of chiral matter at the nanoscale. In particular, the conservation law of optical chirality [23,24] enables the novel physical concept for single-particle enantiomeric recognition presented in this work.

Colloidal dispersions of Au chiral nanopyramids fabricated via high-index off-cut Si wafers—see [12] for all details—are prepared in stabilized solutions with typical NPy sizes of the order of 150 nm. The insets in Fig. 1 show SEM images of such chiral NPys after being stripped off from the Si template, for left and right handedness,

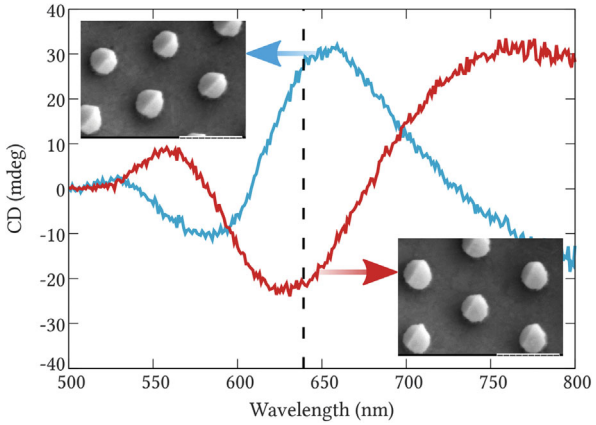

FIG. 1. Circular dichroism (CD) spectra measured through a 1 cm thick cuvette for right-handed (red) and left-handed (blue) NPy dispersions, each prepared in 300 μl of a buffer made of 15 ml 0.1M trisodium citrate dihydrate and 100 μl 0.1M citric acid (pH = 7.32). The dashed line represents the wavelength of the probe laser used in our experiment. The corresponding SEM images of the NPys, taken directly after lift-off, are displayed as insets for the left-handed (left upper corner) and right-handed (right lower corner) NPys. The scale bars are 500 nm.

respectively. A surprisingly strong circular dichroism (CD) signal is measured on these objects, as seen in Fig. 1 [12]. The CD spectra show a clear sign inversion between the two opposite enantiomeric forms of the NPys. Importantly for the experiments, the CD response of the chiral NPys peaks at 639 nm, a wavelength at which a second laser can easily be tuned to and exploited for the chiral recognition protocol described below.

With diameters of ca. 150 nm, the NPys are metallic particles that cannot easily be trapped in three dimensions using a conventional optical tweezer approach [25,26]. To reach good trapping conditions, we built a standing-wave optical trap (SWOT). This enables the axial immobilization of a single metallic nanoparticle at an antinode of the standing-wave pattern created by the reflection of the trapping laser ($\lambda_T = 785$ nm) beam on a mirror placed at a given distance from the beam waist, as depicted in Fig. 2 [27]. For the transverse confinement, the compensation between the Poynting vectors of the incoming and reflected beams leads to a strong reduction of the axial scattering force that can be easily overcome by the gradient force induced by the focusing effect of the objective. The combination of axial and transverse confinements leads to the three-dimensional trapping of the metallic nanoparticle. In such a counter-propagating beam configuration, the scattering forces induced on the nanoparticle therefore stabilize the trap [28]. This is in clear contrast with conventional single-beam optical traps where the scattering forces tend to push away from the waist any metallic particle of a size larger than 100 nm. In addition, as discussed in [29], for instance, the pyramidal anisotropic shape of the NPy is expected to even further enhance the trapping efficiency.

For our experiments, colloidal dispersions of NPys are enclosed in a fluidic cell 120 μm thick. We reduced any electrostatic effects as much as possible by negatively charging the NPys using a citrate buffer solution and the surface of the SWOT end-mirror was dip-coated for 5 min in a 5 wt % polystyrene sulfonate solution. The main constraint for our experiments is the necessity to work with very dilute dispersions appropriate when trapping single NPys. But despite the careful choice of the buffer, the quality of the dispersion evolves in time. NPys tend to adhere on the walls of the fluidic cell, reducing the concentration of the dispersion to levels that cannot be exploited experimentally. This unavoidable effect puts stringent constraints on the time available for repeated experiments on different objects within the same dispersion. In addition, the large surface-to-volume ratio of each NPy leads to the formation of aggregates, in numbers that increase with time. Such aggregates are more likely to be trapped than single NPys and therefore demand a capacity to discriminate between single and aggregated objects. To reach this level of control, we have implemented an interferometric scattering microscopy (ISM) [30]. The setup is described in the Supplemental Material, Sec. A [31], and the method ensures that our experiments involve single NPys, keeping trapped objects only associated with the smallest ISM signals and with diffusive behavior similar to those recorded for single 150 nm Au nanospheres.

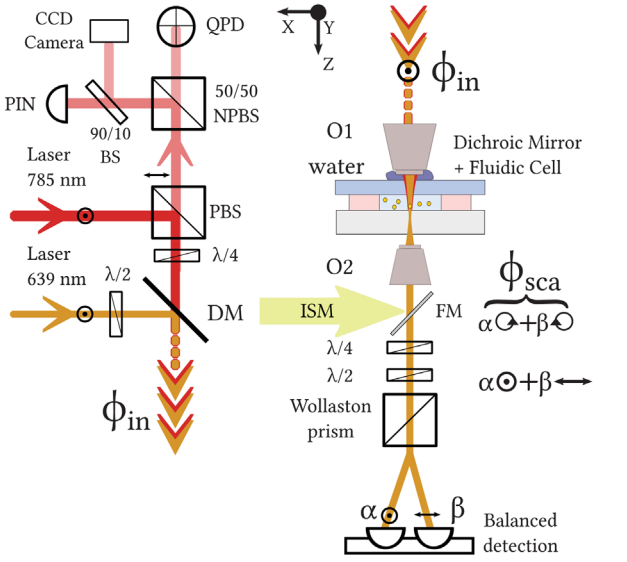

FIG. 2. Scheme of the experimental setup used for trapping a single NPy and for performing chiral recognition on it. The standing-wave optical trap consists of a circularly polarized TEM_{00} beam from a 785 nm diode laser (45 mW) sent into a water immersion objective [O1, 60×, 1.2 numerical aperture (NA)] and focused in a water cell (deionized water, 120 μm thick). The beam is reflected by a dichroic mirror (the end-wall of the fluidic cell) placed at a distance ca. 3 μm from the beam waist, creating a standing-wave pattern within which a single NPy can be trapped. The chiral recognition setup involves a linearly polarized ϕ_{in} probe laser at 639 nm (100 μW) injected inside the trap with a 45° dichroic mirror (DM) and sent through the trap using a dichroic end-mirror. The polarization analysis is performed behind a second (collection) objective (O2, NA 0.6, 40×) on the interfering signal between ϕ_{in} and the field ϕ_{sca} scattered by the single trapped NPy with a $\lambda/4$ quarter-wave plate at 45°, followed by a $\lambda/2$ half-wave plate, and a Wollaston prism. The Wollaston prism separates the incident beam into two linear (vertical and horizontal) polarized beams by an angle of 20°. Both output channels are then sent to a balanced photodetector. The low-power laser beam (594 nm, green trace) for the interferometric scattering microscopy is injected with a flip mirror FM and therefore available throughout the experimental session.

Trapping a single chiral NPy in stable conditions is then done by carefully positioning the end-mirror of our SWOT at a distance of 2 μm behind the waist of the trapping beam. This stability is clearly observed on the power spectral density (PSD) associated with the motion of the trapped NPy in each of the three dimensions displayed in Fig. 3. The Gaussian distribution of the fluctuations in the intensity of the recollected trapping beam, as measured with the *pin* photodiode, clearly demonstrates that the single NPy is well localized in space, i.e., well trapped.

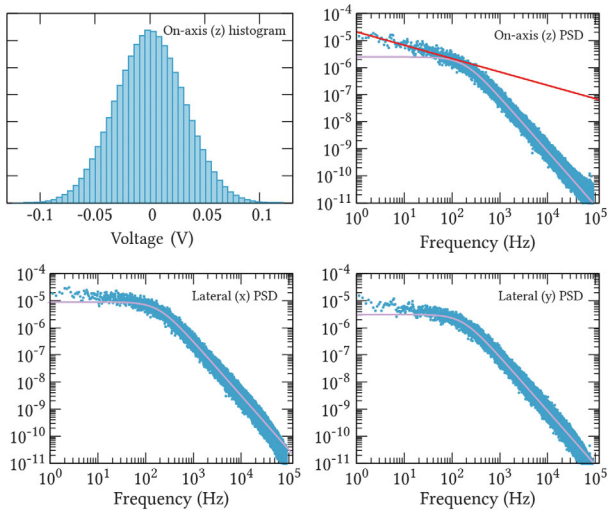

FIG. 3. (a) The intensity histogram along the optical axis shows a Gaussian like distribution of positions. Such behavior is expected for the motion of a single nano-object within a stable optical trap. (b–d) Power spectral densities (PSD) acquired for 36 s along the three x, y, z spatial axes for a trapped chiral NPy. A PSD in blue color is 8× averaged, and the continuous purple curve gives the best Lorentzian fit. (b) PSD along the optical z axis, calculated directly from the intensity of the trapping beam scattered back into the objective and recorded with the *pin* photodiode (see Fig. 2). The red line gives the best fit of the data on the low frequency part of the spectrum (from 1 to 200 Hz) and has a slope of −0.49. (c)–(d) Transverse horizontal x and vertical y signal components are acquired by the quadrant photodiode (see QPD in Fig. 2). They both show an almost Lorentzian shape, the signature of a harmonic trapping potential.

Above the roll-off frequency of the optical trap, the PSDs also precisely match the f^{-2} signature of free Brownian motion. This implies that at such high frequencies the NPy freely diffuses inside the optical trap. Nevertheless, a closer look at the PSDs reveals an interesting deviation below the trap roll-off frequency. The measured PSD indeed departs from the Lorentzian PSD profile expected in the case of a simple harmonic optical trap. This is particularly clear along the optical axis in Fig. 3(a) with a spectral dependence $S_z[f] \propto f^{\alpha}$ $(\alpha \simeq -0.49)$. While this low-frequency power law can slightly depend on the position of the end-mirror when positioned at a distance of about 2 μm behind the waist of the trapping beam, we have checked that we could never record the low-frequency $k_B T/\eta\pi^2$ plateau expected for a Lorentzian PSD measured for a viscous drag η at temperature T. In fact, the ~ -0.5 exponent is the largest exponent we measured, which, remarkably, corresponds to the best trapping conditions for our SWOT. It is beyond the scope of this work to understand exactly this low-frequency deviation. But considering that it lies between the Lorentzian plateau and the $1/f$ shot noise spectral signature, we anticipate that the uneven facets of the NPy diffusing within a limited trap volume (ca. 0.01 μm^3) could be the source for such additional, broadly distributed, correlations in the low-frequency part of the measured scattering signal.

We now exploit a fundamental consequence of the conservation law of optical chirality [23,24]. Upon nonchiral excitation, a lossy, dispersive chiral object selectively dissipates optical chirality and must therefore break, in the scattering, the initial balance in left (σ_L) vs right (σ_R) circular polarizations of the excitation field. This unbalanced scattering is determined in direct relation with the chiral nature of the scattering object, hence its enantiomeric form. This relation leads us to design an enantiomeric recognition protocol that we now describe.

We first model the scattering on a single NPy using simple paraxial circularly dichroic Jones matrices $J^{\pm}$ associated with each of the two NPy± enantiomers with

$$J^{+} = \begin{pmatrix} \alpha & 0 \\ 0 & \beta \end{pmatrix}, \tag{1}$$

$$J^{-} = \begin{pmatrix} \beta & 0 \\ 0 & \alpha \end{pmatrix}, \tag{2}$$

written in the basis of the circularly polarized states (σ_L, σ_R). In this formulation of purely circularly dichroic nano-objects, the absence of mirror symmetry that characterizes the NPy chirality simply corresponds to real $\alpha \neq \beta$ parameters [32].

Illuminated by an incident field linearly polarized $\phi_{\text{in}} = (1/\sqrt{2})(\sigma_L + \sigma_R)$, the NPy scatters a field $\phi^{\pm}_{\text{sca}} = J^{\pm}\phi_{\text{in}}$ in the forward direction with nonequal (α, β) weights in the (σ_L, σ_R) polarizations. In such a framework, our recognition protocol between the ± forms consists in monitoring the time-averaged intensity $S_3^{\pm} = \langle |\phi^{\pm}_{\text{tot}}|^2_L - |\phi^{\pm}_{\text{tot}}|^2_R \rangle$ component of the Stokes vector associated with the total field $\phi^{\pm}_{\text{tot}} = \phi_{\text{in}} + \phi^{\pm}_{\text{sca}}$ transmitted behind the trap. Normalized to $\langle |\phi_{\text{in}}|^2 \rangle$,

$$S_3^{+} = (\alpha - \beta) + \frac{1}{2}(\alpha^2 - \beta^2) = -S_3^{-}. \tag{3}$$

The first term stems from the interference between the incident field and the scattered field. As a consequence of the conservation law of optical chirality, the scattered field is enantioselectively altered, so that the interfering term is proportional to the relative difference $\pm(\alpha - \beta)$ and hence to the circular dichroism of the single ± enantiomer. The second term $\pm(\alpha^2 - \beta^2)/2$ represents the chiral field directly scattered by the trapped NPy. As such, it measures the optical chirality flux, in agreement with the prediction that optical chirality fluxes of opposite signs are generated by chiral objects of opposite handedness [33,34]. The recognition efficiency of our protocol relies in the global sign inversion of S_3 depending on the optically trapped ± enantiomer. For our experiments performed in the visible range, the NPys, with their pockets and tips, behave as

weak light scatterers. This implies that $|\phi_{\rm in}/\phi^{\pm}_{\rm sca}| \gg 1$ so that the recognition essentially operates through the dominant CD contribution.

The experiment is depicted in detail in Fig. 2. It first immobilizes with the 785 nm laser a single NPy enantiomer in a trapping potential made quasiharmonic by carefully adjusting the position of the end-mirror of the SWOT. Then, a second laser, linearly polarized, is inserted inside the trap volume colinearly with the trapping beam. This laser is slightly focused behind the trap, but to avoid exerting any force on the trapped NPy, its power is kept as low as possible (100 μW) with respect to the polarization analysis (see below). To maximize the selective dissipation of optical chirality ($\alpha - \beta$) with respect to handedness, this second laser is tuned to the CD maximum of the NPy at 639 nm, see Fig. 1. With a dichroic end-mirror, our configuration ensures that the 785 nm laser is reflected, creating the SWOT, while the 639 nm laser is perfectly transmitted by the mirror. In this way, we are able to perform the S_3 polarization analysis behind the trap volume by collecting, through an imaging objective (NA 0.6, 40×), the light transmitted and scattered in the forward direction by the NPy. The interference signal is then sent to a photodetector through a polarization analysis stage made of a quarter-wave plate at 45°, followed by a half-wave plate, and a Wollaston prism. Once the polarization analysis is performed, the NPy is released from the trap by blocking the trapping laser, and the trap is reopened after ca. 1 min in order to catch a new NPy which is, in turn, analyzed in the same way.

This procedure is repeated on two different dispersions of opposite enantiomers prepared in identical fluidic cells (identical dichroic mirrors and cover glasses) in the same way (stabilization and concentration). The two samples are analyzed in a sequential manner, following the same polarization preparation and analysis. One advantage of our experimental protocol using a Wollaston prism is that the optical settings (and, in particular, polarization optics) are left untouched when interchanging the fluidic cells. The measurements performed for each cell are repeated three times for validity for each + and − enantiomers. The single NPy trapping condition is carefully verified each time with the ISM method, and only the scattering intensities and imaging signatures corresponding to the smallest, thus single, objects are measured. The results are gathered in Fig. 4.

The averaged values ($\overline{S_3^+} = -39 \pm 4$ mV and $\overline{S_3^-} = 28 \pm 6$ mV) clearly show that the + and − enantiomeric signals can be distinguished through the polarization analysis. The reproducibility of the S_3 measurements for different NPys trapped from one given dispersion and within the same optical landscape suggests a constant equilibrium position of the NPys inside the optical trap. Despite this, the recorded values do not display the exact sign inversion in the S_3 component between the two

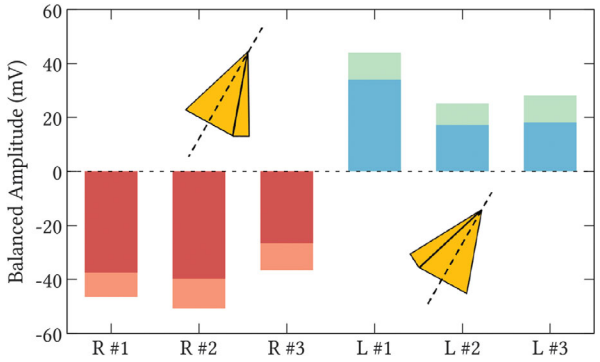

FIG. 4. S_3 Stokes measurements for two dispersions of chiral NPys of opposite handedness. The red bars correspond to different chiral right + NPy labeled from 1 to 3 while the blue bars are three different left − enantiomers. Errors, given by the lighter top of each bar, represent the standard deviation in measuring the S_3 parameter of each trapped NPy. The signal clearly exhibits nonoverlapping intensity differences between the ± enantiomers. We use a fast oscilloscope to measure all S_3 values, averaging over an acquisition time of $\delta t = 50$ μs. Each measurement sequence for a given dispersion is performed in less than 15 min, and the entire comparative study was shorter than 30 min. These requirements are important in order to avoid fluidic drifts and NPy aggregation to affect the stability of the setup.

enantiomers expected from Eq. (3). As discussed in Supplemental Material, Secs. B and C [31], we explain this from (i) the fact that the NPys adopt a preferred orientation inside the optical trap, and (ii) from residual alignment errors in the polarization preparation and analysis stages. We show that these effects only offset the $S_3^{\pm}$ values by the same constant quantity, independently from the enantiomeric form. The central quantity therefore to be monitored is the difference $\Delta_{S_3} = \overline{S_3^+} - \overline{S_3^-}$ for which the deviation from zero directly measures the NPy's preferential dissipation of incident left- or right-handed circularly polarized light, i.e., the NPy circular dichroism $\propto (\alpha - \beta)$.

Two additional sources of variations can also be accounted for. First, small structural changes between NPys successively trapped induce distributions in the values for α, β. Then, NPy thermal diffusion inside the optical trap leads to intensity variations (via the Gaussian distribution of the trapping beam intensity) and depolarization in the forward scattering associated with an error of ∼5 mV in the balanced detection for every trapped enantiomer. Such differences eventually limit the discrimination sensitivity of the experiment, but despite these, our setup allows us to unambiguously measure for single NPy enantiomers $\Delta_{S_3} = -67 \pm 10$ mV, well above all data deviations. We stress once again that this result is acquired on single chiral nano-objects, optically probed while diffusing within the optical trap.

Considering the few remarkable experiments that have been performed at the micrometer scale [20,21,35] or with two-dimensional objects [34,36], our demonstration of

stable optical trapping of single chiral nano-objects in three-dimensions is an important step in the development of new experimental methods for controlling and manipulating chiral nano-objects [37]. The concomitant capacity of our optical tweezer for *in situ* chiral recognition gives the possibility to perform chiroptical studies on single artificial chiral objects at the nanometer scales with an unprecedented level of control. The possibility to selectively manipulate chiral matter via new modes of actuations is key for pushing the applicative potential of all-optical strategies in the vast and cross-disciplinary realm of chirality.

This work was supported by Agence Nationale de la Recherche (ANR), France, ANR Equipex Union (Grant No. ANR-10-EQPX-52-01), the Labex NIE projects (Grant No. ANR-11-LABX-0058-NIE), and the Swiss National Science Foundation under Award No. 20021-146747. Y. R.-C. is a member of the International Doctoral Program of the Initiative d'Excellence (PDI-IDEX) of the University of Strasbourg, which support is acknowledged.

*genet@unistra.fr

[1] A. Ben-Moshe, B. M. Maoz, A. O. Govorov, and G. Markovich, Chem. Soc. Rev. **42**, 7028 (2013).
[2] V. K. Valev, J. J. Baumberg, C. Sibilia, and T. Verbiest, Adv. Mater. **25**, 2517 (2013).
[3] S. Boriskina and N. I. Zheludev, *Singular and Chiral Nanoplasmonics* (CRC Press, Boca Raton, FL, 2014).
[4] Y. Tang and A. E. Cohen, Phys. Rev. Lett. **104**, 163901 (2010).
[5] R. Tullius, A. S. Karimullah, M. Rodier, B. Fitzpatrick, N. Gadegaard, L. D. Barron, V. M. Rotello, G. Cooke, A. Lapthorn, and M. Kadodwala, J. Am. Chem. Soc. **137**, 8380 (2015).
[6] M. Alizadeh and B. M. Reinhard, ACS Photonics **2**, 942 (2015).
[7] K. M. McPeak, C. D. van Engers, S. Bianchi, A. Rossinelli, L. V. Poulikakos, L. Bernard, S. Herrmann, D. K. Kim, S. Burger, M. Blome *et al.*, Adv. Mater. **27**, 6244 (2015).
[8] M. Schäferling, *Chiral Nanophotonics: Chiral Optical Properties of Plasmonic Systems*, Vol. 205 (Springer, New York, 2016).
[9] S. Meinhardt, J. Smiatek, R. Eichhorn, and F. Schmid, Phys. Rev. Lett. **108**, 214504 (2012).
[10] A. Nourhani, V. H. Crespi, and P. E. Lammert, Phys. Rev. Lett. **115**, 118101 (2015).
[11] D. Schamel, M. Pfeifer, J. G. Gibbs, B. Miksch, A. G. Mark, and P. Fischer, J. Am. Chem. Soc. **135**, 12353 (2013).
[12] K. M. McPeak, C. D. van Engers, M. Blome, J. H. Park, S. Burger, M. A. Gosálvez, A. Faridi, Y. R. Ries, A. Sahu, and D. J. Norris, Nano Lett. **14**, 2934 (2014).
[13] J. Yeom, B. Yeom, H. Chan, K. W. Smith, S. Dominguez-Medina, J. H. Bahng, G. Zhao, W.-S. Chang, S. J. Chang, A. Chuvilin *et al.*, Nat. Mater. **14**, 66 (2015).
[14] C. Bechinger, R. Di Leonardo, H. Löwen, C. Reichhardt, G. Volpe, and G. Volpe, Rev. Mod. Phys. **88**, 045006 (2016).
[15] X. Li and M. Shapiro, J. Chem. Phys. **132**, 194315 (2010).
[16] D. V. Guzatov and V. V. Klimov, Quantum Electron. **41**, 526 (2011).
[17] A. Canaguier-Durand, J. A. Hutchison, C. Genet, and T. W. Ebbesen, New J. Phys. **15**, 123037 (2013).
[18] R. P. Cameron, S. M. Barnett, and A. M. Yao, New J. Phys. **16**, 013020 (2014).
[19] S. Wang and C. Chan, Nat. Commun. **5**, 3307 (2014).
[20] Y. Zhao, A. Saleh, M. Van de Haar, B. Baum, J. Briggs, A. Lay, O. Reyes-Becerra, and J. Dionne, Nat. Nanotechnol. **12**, 1055 (2017).
[21] G. Cipparrone, A. Mazzulla, A. Pane, R. J. Hernandez, and R. Bartolino, Adv. Mater. **23**, 5773 (2011).
[22] G. Tkachenko and E. Brasselet, Nat. Commun. **5**, 3577 (2014).
[23] L. V. Poulikakos, P. Gutsche, K. M. McPeak, S. Burger, J. Niegemann, C. Hafner, and D. J. Norris, ACS Photonics **3**, 1619 (2016).
[24] G. Nienhuis, Phys. Rev. A **93**, 023840 (2016).
[25] K. Svoboda and S. M. Block, Opt. Lett. **19**, 930 (1994).
[26] P. M. Hansen, V. K. Bhatia, N. Harrit, and L. Oddershede, Nano Lett. **5**, 1937 (2005).
[27] G. Schnoering and C. Genet, Phys. Rev. E **91**, 042135 (2015).
[28] P. Zemánek, A. Jonáš, L. Šrámek, and M. Liška, Opt. Lett. **24**, 1448 (1999).
[29] O. Brzobohtý, M. Šiler, J. Trojek, L. Chvàtal, V. Karàsek, and P. Zemànek, Opt. Express **23**, 8179 (2015).
[30] K. Lindfors, T. Kalkbrenner, P. Stoller, and V. Sandoghdar, Phys. Rev. Lett. **93**, 037401 (2004).
[31] See Supplemental Material at http://link.aps.org/supplemental/10.1103/PhysRevLett.121.023902 for a description of the interferometric scattering microscopy implemented in this work, Sec. A, a discussion on the influence of fixed orientations of the nanopyramids inside the optical trap, Sec. B, and an evaluation of residual alignment errors in polarization preparation and analysis stages, Sec. C.
[32] A. Drezet and C. Genet, in *Singular and Chiral Nanoplasmonics*, edited by S. Boriskina and N. I. Zheludev (Pan Stanford Publishing, Singapore, 2014), Chapter 4.
[33] L. V. Poulikakos and D. J. Norris (in preparation).
[34] L. V. Poulikakos, P. Thureja, A. Stollmann, E. De Leo, and D. J. Norris, Nano Lett., DOI: 10.1021/acs.nanolett.8b00083 (2018).
[35] G. Tkachenko and E. Brasselet, Nat. Commun. **5**, 3577 (2014).
[36] E. Vinegrad, D. Vestler, A. Ben-Moshe, A. R. Barnea, G. Markovich, and O. Cheshnovsky, ACS Photonics **5**, 2151 (2018).
[37] Y. Zhao, A. A. Saleh, and J. A. Dionne, ACS Photonics **3**, 304 (2016).